Fatigue Anisotropy in Cross-Rolled, Hardened Medium Carbon Steel Resulting from MnS Inclusions

CORNELIUS TEMMEL, BIRGER KARLSSON, and NILS-GUNNAR INGESTEN

Anisotropy of forged steel components is especially adverse when it concerns rotationally symmetric components. Manganese sulfides (MnS) in steels may be desired for their improvement of machining properties; however, they also deteriorate fatigue behavior. A quantification of the effect of MnS on anisotropy is necessary to find an optimum for component dimensioning. To isolate the influence of MnS on anisotropy only, high cleanness of the test material is required. The test material in the current investigation was molten in a vacuum furnace to high-cleanness composition. Materials with two different S levels were produced to detect variations in anisotropy according to amount, shape, and distribution of the MnS inclusions. The two batches were cross-rolled to plates with a deformation ratio of 4.5. The MnS phase constitutes, upon forging or rolling, pancake-shaped inclusions. In the case of cross-rolling, an in-plane rotational symmetry of the inclusions could be created. The shape and size of these inclusions are essential for the mechanical behavior of the material. Push–pull fatigue testing was performed in longitudinal (in plane) and short transversal directions relative to the rolling plane. The results showed strong anisotropy of the fatigue behavior with inferior performance in short transverse directions where the principal stress is perpendicular to the flattened inclusions. The anisotropy was somewhat more pronounced for the high-S material, resulting from a different fatigue crack growth mechanism.

I. SULFIDE INCLUSIONS AS A REASON FOR ANISOTROPY

A. *Anisotropy*

FORGED materials generally show directional material behavior. This behavior is especially adverse when isotropic properties are required, as in, for example, most rotationally symmetric components. An example of such a component would be a transmission gear wheel that is die forged from a fraction of a billet. Anisotropy is introduced in the material by not only component forging and deformation operations but also earlier during the manufacturing process of the material such as, for example, continuous casting. The orientation of the billet is superimposed by the orientation created during either horizontal or vertical die forging of the material.

Anisotropy of any kind, but especially mechanical anisotropy, arises from the four types of orientation of a microstructure that can be distinguished. Those four types are (1) crystallographic texture (preferred crystal orientation), (2) elongated grains, (3) banded (two)-phase structure, and (4) elongated inclusions.

B. *Inclusions*

Elongated inclusions have for fatigue anisotropy a major and superimposing effect because inclusions constitute with their characteristic as stress concentration factor a dominating site for fatigue crack initiation.[1–4] The criticality of inclusions as stress concentrators changes with their size and shape,[5,6] but also with their ability to bond with the matrix material.[7] An inclusion that cannot maintain bonding forces to the matrix material might behave just like a pore or crack within the material. An inclusion with proper bonding to the surrounding material is as a microstructural constituent less lethal to mechanical properties, and the material thus exhibits more ductility.

It has been shown that inclusions are accountable not only for fatigue anisotropy, but they also dominate all mechanical anisotropy (such as tensile strength, ductility, fracture toughness, *etc.*).[1,3,4] Orientation of inclusions potentially governs directional behavior of a material.[1,7] To diminish inclusion anisotropy, several approaches can be considered. Anisotropy can be controlled by changing parameters such as shape, amount, and dispersion of inclusions. Those changes can be achieved by interalia variation of deformation temperature and deformation ratio of the material.[5,8] Also, changes in material composition chemistry might alter inclusions in a beneficial way (*i.e.,* diminish the mechanical anisotropy).[3]

Sulfides represent the largest indigenous inclusions in steel. Therefore they deserve special interest.

C. *Sulfides*

The most frequent and also most important sulfide inclusions in modern steels are of manganese sulfide (MnS) type.[9] Therefore, the focus in this paper is on MnS. MnSs in structural steels are appreciated as constituents for their beneficial role during machining. Machining of free-cutting steel represents a large fraction of the production cost of a component. MnSs in the component material help to save machining costs by chip embrittlement, tool protection, and flow zone improvements.[2] Because MnSs and their adverse behavior as steel inclusion cannot be avoided, a compromise has to be found to satisfy both component

CORNELIUS TEMMEL, Researcher, and NILS-GUNNAR INGESTEN, Manager Forged Materials, are with Materials Technology, Volvo Powertrain Sweden, Göteborg, Sweden. Contact e-mail: cornelius.temmel@gmx.net BIRGER KARLSSON, Professor, is with the Department of Materials and Manufacturing Technology, Chalmers University of Technology, Göteborg, Sweden.

Manuscript submitted December 14, 2005.

strength as well as machinability. Three different types of MnS can be distinguished.[9] They appear according to Al content, which is used to deoxidize the steel. The solubility of S in liquid steel increases with decreasing O content. For machining purposes, MnSs that can act as stress raisers in the shear plane at the tip of the tool are to be favored. Because of their comparatively smaller dimensions, type II MnS inclusions are inferior to MnS types I and III.[9] MnSs improve machinability best for low to medium cutting speeds.

Ca-treated steels show improvements not only in machinability, but also in mechanical properties. By deoxidizing steel with Ca, Ca-rich oxides form that improve machinability, especially at high cutting speeds, such as when using cemented carbide tools. Furthermore, Ca additions lead to more rounded MnS inclusions, which promote isotropic mechanical behavior.[2] The three types of MnS inclusions are MnS type I, MnS type II, and MnS type III.

1. *MnS type I*

Type I is globular with a wide range of sizes. It is formed in rimmed or semikilled steel, in which the O content of the liquid steel is high and the S solubility low, resulting in a precipitation of sulfide at a comparatively high temperature. Type I is usually present in multiphase inclusions.

2. *MnS type II (grain boundary sulfide)*

Type II is found in killed steels, thoroughly deoxidized with Al but without excess and where the O content is low. As a consequence, these steels have a high S solubility and the sulfide phase precipitates late during the last parts of the steel ingot to solidify. Therefore, the type II sulfide is found in the primary grain boundaries in a dendritic pattern.

3. *MnS type III*

Type III is irregular, often angular in shape, and is randomly distributed in the steel. It has no marked difference to type I, although it always forms monophase inclusions. Type III is frequently found in steels deoxidized with an excess of Al. The O content of the liquid is low, but the S solubility is also low compared with steels forming type II sulfides, because of to the high Al content in solution in the liquid steel.

4. *Properties of MnS*

MnSs appear as α-MnS in steel in a cubic crystal lattice. Their density is approximately 3.99 g/cm^3. The melting point lies at 1655 °C. The hardness at ambient temperature of pure MnS is 170 HV. By solid solution hardening with other metals such as Cr, Ni, V, Ca, etc., or with O, the hardness can be increased to levels of around 400 HV.[3,9] Matsuno *et al.* [10] present results confirming an increase in nominal yield strength for MnS resulting from solid solution hardening. The hardness of MnS decreases almost linearly with increasing temperature, and at 1000 °C only one tenth of the initial hardness is left.[10]

5. *Deformation of MnS*

MnSs will have, different from other inclusions such as oxides or silicates, the (lethal) property to be softer than the steel matrix material. This has importance for deformation operations of the steel, in which MnS inclusions of type I and type III might deform to a flat pancake shape. Type II MnSs, with their dendritic appearance, are rotated into the deformation plane. Still, local similarities to a pancake shape can be seen. The consequence of pancake or discoid shapes is high stress concentrations on those sharp edges of the deformed MnS[1] and strong material anisotropy.

6. *Deformation of the matrix*

The deformation ratio of the material has a direct influence on the dispersion and on the size and shape of the inclusions as well. The higher deformation ratio applied, the finer the inclusions are dispersed.[5] With ''controlled'' hot rolling, inclusion dispersion can be managed.[3]

7. *Shape control of MnSs by solid solution hardening*

Strong deformation of MnSs, especially into a pancake shape with a high stress intensity factor at the small radii, should be avoided to diminish anisotropy in the material. One strives to keep the inclusions as spherical as possible so as not to introduce orientation effects.

Inclusions will deform little, or not at all, if they have a hardness twice as great as the matrix.[3] This cannot be achieved for MnSs, but there are several mechanism to obstruct sulfide deformation. As mentioned earlier, solid solution strengthening is appropriate to maintain the spherical shape of the S inclusions. Additions of Cr, Ni, V, O, and the strong sulfide former Ca increase inclusion strength and diminish plasticity of the sulfide inclusion. Also, the addition of rare earths (Ce, La, Nd, etc.) is beneficial in this matter.[2,3,11,12] The increase in inclusion strength will result in less deformation of the inclusions upon material working.

When alloying MnS with elements such as those mentioned earlier to achieve solid solution hardening, it has to be considered that the surrounding matrix material and its properties will be influenced as well. Kiessling and Lange[9] cite an example in which the steel contained 1.52 wt pct Cr in the matrix material and 5 wt pct in solid solution in the MnS. Increasing the Cr content in the steel to 18.1 wt pct raises the Cr content in the MnS to 26 wt pct. A 20-wt pct increase of Cr as solid solution in MnS doubles the hardness of the inclusion from initially ~170 to ~350 HV. An analogous increase of Cr in the matrix material creates a wholly new material.

Ca is a popular addition to modify inclusion chemistry and morphology such that inclusions maintain globular shape better, even during hot working. Appropriate results can be reached with as little as 1 pct Ca in solid solution in the MnS.[3] Ca, having a strong affinity to S, will prefer bonding to S rather than alloying the matrix material. The total amount of Ca used in Ca-treated steels is typically less than 50 ppm. It has to be mentioned that the benefits of Ca are not bound to only solid solution strengthening of sulfides. Also, formation of CaS sometimes in combination with CaO can, when efficient calcium treatment is practiced, produce benefits. Generally, Ca treatments of steels are complex. We recommend reading the study by Wilson.[13]

8. *Shape control of MnS by temperature management*

At higher working temperatures, the deformability of the matrix material often increases more rapidly than that of the MnS inclusions.[5] Therefore the term *relative plasticity*

is defined as the ratio of inclusion true strain to overall matrix true strain.[8] At lower relative plasticity it will be more difficult to change the shape of the inclusions at, up to a certain limit, higher temperatures. This means that the original shape of MnS can be somewhat maintained more easily at higher working temperatures, thus lowering the level of anisotropic material behavior. Baker *et al.*[8] have experimentally determined the temperature regime in which relative plasticity is lowest and MnS inclusions withstand deformation best. It turns out that this is at ~700 °C, when the transformation of ferrite to austenite starts. Little deviation from this temperature produces much worse results. At temperatures of ~800 °C, the relative plasticity shows a peak that declines with increasing temperatures up to 1200 °C.

Change of shape in MnSs can also be accomplished by heat treatments that cause "spheroidization." Leslie[3] cites two experiments in which steel (0.39 pct C, 0.55 pct Mn, 1.7 pct Ni, and 0.75 pct Cr; 85 pct reduction) was exposed to 1310 °C for 1 hour, and dual-phase steel (1.40 pct Mn and 0.011 pct S; 99 pct reduction) was held at 980 °C for 2 hours. Both experiments obtained complete spheroidization of the MnSs. However, it remains to be seen what improvement in mechanical properties can be obtained and at what cost.

9. *Residual stresses around MnS*

Because of their larger coefficient of thermal expansion, MnSs introduce during and after cooling (after, for example, a hot working operation) compressive residual stresses into the surrounding matrix material. These compressive circumferential stresses are seen to have a positive effect on the fatigue properties[2,3]—only, however, if the bonding between inclusion and matrix is strong enough to carry the emerging radial tensile forces between inclusion and matrix surface, which consequently leads to compressive stresses in a circumferential direction in the matrix around the inclusion. This circumferential compression may prevent crack growth starting from the inclusion. Brooksbank and Andrews[14] believe that MnSs contract away from the interface, thereby forming voids upon cooling rather than compressive circumferential stresses in the matrix.

10. *Bonding between MnS and steel matrix*

MnS–steel matrix bonding suffers as a result of the greater shrinkage of the inclusion during cooling. Parting can occur even without plastic straining of the material,[15] or with very little plastic strain. Brooksbank and Andrews[15] suggest that microvoids could form around inclusions of that type already during heat treatments. They rate MnS as "nondetrimental" (possibly beneficial) with the highest "void-forming potential" compared with other inclusions such as aluminates, alumina, silicates, and oxides. Furthermore, the interface between the steel matrix and MnS attracts surface active elements, such as S, H, and P, which might weaken the interface as well. Addition of Cr or Mo can enhance the cohesion between ferrite and MnS,[3] but changes in chemical composition have to be considered for the matrix material as well.

D. *Fatigue behavior*

Fatigue failure is closely linked to inclusions. For high-cycle fatigue (HCF), nearly all cracks originate from inclusions.[1–3,16] Again, type, shape, size, and volume fraction of inclusions have a crucial influence on component behavior.

The orientation of inclusions will strongly promote anisotropy. The deformable MnSs are especially hazardous because they might form, upon forging, very narrow cavities that result in very high stress concentrations.[1] For cyclicly loaded components, failure consists of fatigue crack initiation, fatigue crack propagation, and final rupture.

1. *Fatigue crack initiation*

Defects, such as inclusions, pores, and voids often act as stress concentrators. Therefore, these defects can ease crack initiation considerably in such a way that fatigue failure can occur at low stress amplitudes. A critical inclusion size is necessary for fatigue crack initiation, which is dependent on the surrounding matrix and on the type of loading.[2] Correspondingly, this critical size begins in the single-micrometer regime, which is exceeded by most indigenous inclusions.

Inclusions can generate stresses within the surrounding matrix material. These stresses arise after material working or heat treatments. For heat treatments, the thermal expansion coefficient is crucial. Inclusions with lower coefficients than the iron matrix are most damaging because they introduce a zone of residual circumferential tensile stresses within the steel matrix around the inclusion. MnSs are often beneficial, because they introduce, as a result of their larger expansion coefficient, compressive circumferential stresses.[2,3,7,15] High stresses around inclusions, also during material processing, can force phase transformations in the matrix material (such as transformation of retained austenite to martensite), thus contributing to fracture behavior.[7]

The stress state around an inclusion will highly influence crack initiation. The stress is determined by particle size and shape, residual stresses, inclusion orientation, and so on. Failure evokes from exceeding a limit. This limit can be material plastification at the highest stressed site, but also debonding of the matrix–inclusion interface. Debonding can occur at stresses below the fatigue limit.[3]

2. *Fatigue crack propagation*

The effect of inclusions on fatigue crack growth is less pronounced than on fatigue crack initiation.[3] At higher volume fractions of inclusions, it is likely that another inclusion is present within the plastic zone surrounding a crack tip. If this inclusion is bonded weakly to the matrix, it will generate a strain field and thus contribute to crack propagation.[1]

Fatigue life length can be improved by a reduction of inclusion volume fraction and inclusion size, and by a decrease of microstructural orientation.[3,4] However, Härkegård[16] concludes in his paper that the volume fraction of inclusions has a relatively smaller effect on fatigue behavior compared with the influence on the ductility of a material.

II. CHOICE OF SUITABLE MATERIAL FOR ACTUAL COMPONENTS

Production material for power transmission components in vehicles often contains high S levels of typically 0.04 wt pct. This is to promote MnS formation and therewith increase

the machinability of the component. Apart from all the benefits that arise from MnS, there is also the strong potential of introducing mechanical anisotropy upon deformation mechanisms. Indeed, forged gears show strong directional dependency, especially for the fatigue strength of single teeth.

For the current investigation, it was of interest to quantify that influence of MnS on fatigue properties. Two materials, differing only in S levels, were compared for their fatigue response under previously described conditions. The material with the higher S content is in accordance with production material. Through-hardening steel was chosen to simulate case properties of case-hardened steel components. To verify anisotropic behavior, two test directions were chosen: one perpendicular to and one aligned with the deformation axis. However, deformation grades could only reach relatively limited values compared with those found in heavy working in practice.

III. EXPERIMENTAL DETAILS

A. *Material*

A test material corresponding to 42CrMo4 steel (EN 10083-1) was chosen. Restrictions on cleanness of the steel were high (Table I) to avoid contaminations such as oxides, silicates, and so forth. Equal chemistry with two different S levels (high S = HS and low S = LS) was required to compare their influence. Such material had to be custom cast in a vacuum furnace according to our specifications in amounts of two 54-kg ingots. The S content of the HS material corresponds to the S content of the 42CrMo4 steels used in production for transmission gear wheels, whereas the other material has a considerably lower S level (Table I).

To generate deformation in the material, the ingots were cross-rolled. Cross-rolling was chosen to imitate a forging operation that would have been difficult to accomplish. According to a rolling pass schedule, the ingots had been deformed to final plate shape after heating them to 1200 °C. The cross-rolling should deform the soft MnS inclusions to a pancake shape. The original ingot (length, 350 mm; 150 mm square tapering to 140 mm square) was reduced to a plate with a deformation ratio of ~4.5. The final thickness of the plate was 30 mm. The intention was thus to create a microstructure with in-plane isotropy.

For further preparation of the material to investigate, the directions on the rolled plates had to be defined as L (longitudinal), T (transverse) and S (short transverse; Figure 1[17]). The two types of push–pull fatigue samples have as their rotation axis the direction S and L respectively. Specimens with an axis in direction T were not tested because they were expected to show similar results as samples with axis in direction L.

B. *Microstructural Description*

The microstructure of the cross-rolled material was ferritic–pearlitic. Electron backscatter diffraction investigations showed random crystallographic orientations. Upon hardening, the microstructure transformed to martensite. Macro-orientation of the material was then made visible with etching in picric acid. This orientation originates from the dendritic cast structure, which was layered when cross-rolled. Both the LS and HS material showed similar appearance (compare with Figure 2). It was assumed that no crystallographic orientation did develop upon hardening.

The MnS population of the HS as well as of the LS material was described according to ASTM E 1245-03[18] (compare with Table II). Large standard deviations reflect the fact that the MnSs were of type II. MnS characteristics as seen in the HS material can also be found in gear wheel production material.

The MnSs were predominately found in the last solidified material, which implies a stacked appearance of the sulfides. The last solidified material can be identified as the areas with dark contrast in Figure 3.

C. *Tensile Properties*

Tensile tests of the material were carried out on tensile test specimens of 80 mm in length (according to Volvo standard 1024,213) oriented in the L direction. The material was hardened and tempered to 450 HV30. The ultimate tensile strength (R_m), yield stress ($R_{p0.2}$), elongation (A_5), reduction of area (Z), and Young's modulus (E) can be learned from Table III.[19] Obvious is the more brittle behavior of the HS variant, which correlates with its higher inclusion content.

S and L tests of the HS material were compared on 30-mm miniature specimens[20] that showed analog behavior up to the yield stress (~1400 MPa). However, the ductility of the S direction suffered from the inclusions orientation, so that the specimen fractured soon after reaching the yield stress.

D. *Fatigue Specimen Preparation*

The two plates (LS and HS material) were cut according to Figure 1, which shows the LS material (accordingly for HS material). Each plate produced 48 samples for push–pull fatigue testing, 24 of which were in the S direction and 24 were in the L direction. Consequently, four different series could be tested: HS-L, HS-S, LS-L, LS-S. The blanks for the L push–pull samples measured ~90 × 30 × 30 mm;

Table I. Specification for the Chemical Composition

Element	S (LS)	S (HS)	C	Si	Mn	Cr	Mo	O	P	N	Sn	Al	V	Cu
Spec. (wt pct)	0.002	0.045	0.38–0.45	≤0.40	0.60–0.90	0.90–1.20	0.15–0.30	<0.002	<0.02	<0.005	<0.01	<0.01	<0.05	<0.01
Result LS	0.004	—	0.43	0.23	0.74	1.05	0.22	27 ppm	0.004	0.005	0.002	<0.005	0.004	<0.01
Result HS	—	0.042	0.43	0.24	0.76	1.06	0.23	15 ppm	0.004	0.002	0.002	<0.005	0.004	<0.01

LS is-the low-S material; HS is the high-sulfur material. Results for oxygen content from OVAKO. All other results from Volvo analysis.

the blanks for the S samples, ~30 × 30 × 30 mm. End tab material was inertia welded to the S blanks to increase dimensions to sufficient length. Both the L as well as the S blanks were turned into push–pull specimens according to Figure 4. The test specimens were through-hardened to a final hardness of ~450 HV30. For this purpose, the samples were austenitisized at 850 °C for 45 minutes in a nitrogen–methanol–propane atmosphere, followed by quenching in an oil bath at a temperature of 120 °C. Tempering was carried out at 400 °C for 1 hour. Subsequently the specimens were polished to a 1-μm smoothness at the center waist area. Polishing should diminish surface influences during fatigue testing as well as enable high-quality graphic documentation.

E. *Fatigue Tests*

HCF testing was carried out on an Amsler resonance fatigue test machine at ~215 Hz. The peak load was cycled at a load ratio of $R = -1$, where a drop of 5 pct in maximum load was defined as the failure criterion. Specimens were rated survivors when they reached the limit of 10 million cycles. The testing was conducted in accordance with the staircase method (up-and-down method according to Dixon and Mood[21]). The initial stress amplitude level at which the staircase method should be used was determined by the first specimen of each series. The first specimen was tested at a conservative stress amplitude until failure or until it reached run-out at 10 million cycles. If a run-out occurred, the stress was increased by one step. The same sample was then retested until it fractured. The fracture stress of this first specimen would then be the starting stress for the staircase method.

The step size chosen was 15.72 MPa (1 kN). Several specimens were, for practical reasons, tested with a step size of 7.86 MPa (0.5 kN).

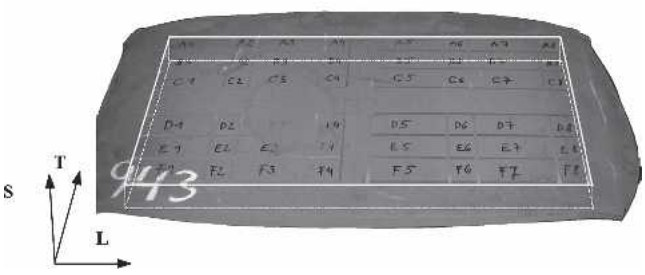

Fig. 1—Indexing of directions on the rolled plate according to ASTM E 399[17] (here, low S material). Sections of microsamples are named after the direction of the normal of the section (compare with Figure 2).

IV. RESULTS

Fatigue data for LS-S, HS-S, LS-L, and HS-L specimens are presented in Figures 5 and 6. The test results of all specimens of each series can be embraced in fairly narrow scatter bands.

The graphs have been modified so that several data points show no background color. Such a modification of a data point had one of the following three reasons. First, fractures emanate from an abnormally large inclusion (see Figure 14 and compare it with Figures 5 and 6). Inclusions of that size should not appear in commercial steels. However, these specimens contributed to the staircase method by influencing the test sequence. To calculate the mid value and the standard deviation for the results of the staircase method according to Dixon and Mood,[21] these fractures were considered as well.

Second, specimens are marked differently because they had a history of retests. A retest on a specimen was carried out either with the intention of finding an appropriate initial load level for each series or after surviving a test at low stress (as did five specimens of the LS-L series). The specimens determining the initial stress level did contribute to mid-value and standard deviation calculations. The five retested specimens of the LS-L series did not contribute

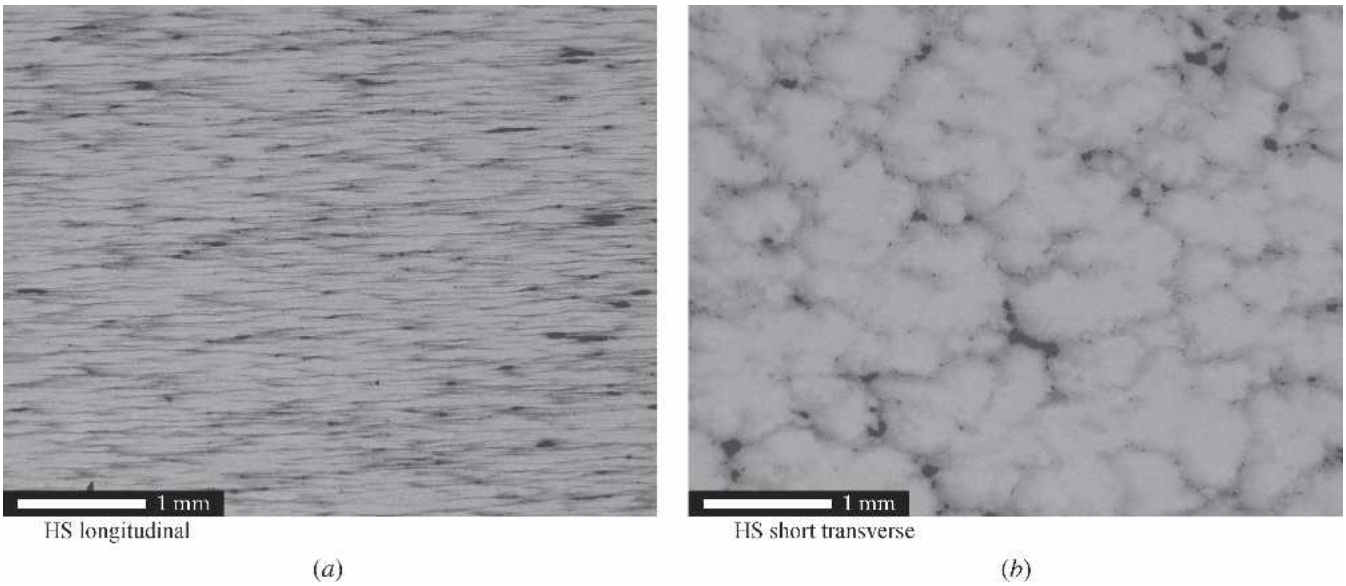

Fig. 2—Macrostructure of the hardened test material etched in picric acid. A distinct macrostructural difference in orientation can be seen for the high S (HS) material. The longitudinal direction is shown in (*a*) whereas the short traverse direction is shown in (*b*). Analog for the low S material.

to mid values and standard deviations. Furthermore, they were tested independently of the staircase cycle for the series LS-L. However, the test load for these five specimens was chosen according to their history and the result of the previous retested sample.

Third, some single specimens experienced thread fractures. These samples were taken out of the testing sequence and they did not contribute to mid-value and standard deviation calculations or to the staircase procedure.

The significance of all those specimens with modified data points as test results is questionable. Therefore, these samples were not approved to appear in the ''collected results'' (Figure 7).

A. *LS-S and LS-L*

Figure 5 indicates the fatigue test results of the LS-S and the LS-L series. Figure 5 also contains additional information on five retested specimens that previously were survivors. These five specimens did not contribute to the mid-value calculation or to the staircase method. Specimens were retested when the initial load level to which they were exposed seemed low enough not to influence a second test markedly at a considerably higher load. Retested specimens either survived a second test or fractured and thus gave information on a load–lifetime relation. The exposure to the initial (low) load was a result of a misjudgment of the fatigue strength level to be expected.

Although all 23 data points were used for mid-value and standard deviation calculation of the LS-S series, only the last 14 were used for the LS-L series. This is because the first nine specimens were tested at too low a load (some of which were retested later, as mentioned earlier).

Table II. ASTM E 124503 Rating of MnS Inclusions in high S in (HS) and low S (LS) Material

		λ (mm)	Length (μm)	Width (μm)	Aspect Ratio
LS	Mean	12.29	2.03	1.21	1.9
	SD	—	0.81	0.47	1.3
HS	Mean	0.35	4.83	1.26	3.8
	SD	—	4.74	0.75	2.6

λ is the mean free path between neighboring inclusions measured as the edge-to-edge distance between inclusions in the through-thickness direction [19]. ''Mean'' is the calculated mean values.

B. *HS-S and HS-L*

Figure 6 shows the fatigue test results of the HS-S and the HS-L series. Although we used all 23 data points for the mid-value and standard deviation evaluation for the HS-S series, only the last tested 13 points were used for the HS-L series. This is because a single step size change from 7.86 to 15.72 MPa (0.5 to 1 kN) for one specimen (test 10) would falsify the calculation. The hypothetical values for the consideration of all tested 20 data points (3 of the 23 specimens experienced thread failure) are also given in Table IV. These hypothetical values were calculated with a persistent step size of 7.86 MPa (0.5 kN).

Mid values and standard deviations are given in Table IV for the LS-S, LS-L, HS-S, and HS-L series. The values were calculated according to the Bruceton method described i.a. by Dixon and Mood.[21] Each calculated mid value can be understood as the fatigue limit of the corresponding tested series. This assumption is adequately accurate, because the chosen stress amplitudes oscillate, conforming to the staircase method, around the fatigue limit of the material.

C. *Collected Test Information*

The collected test data of all four series is given in Figure 7. It contains all relevant fatigue test data that are accepted as unquestionable results. The graph does not contain information on retested specimens or specimens that were not

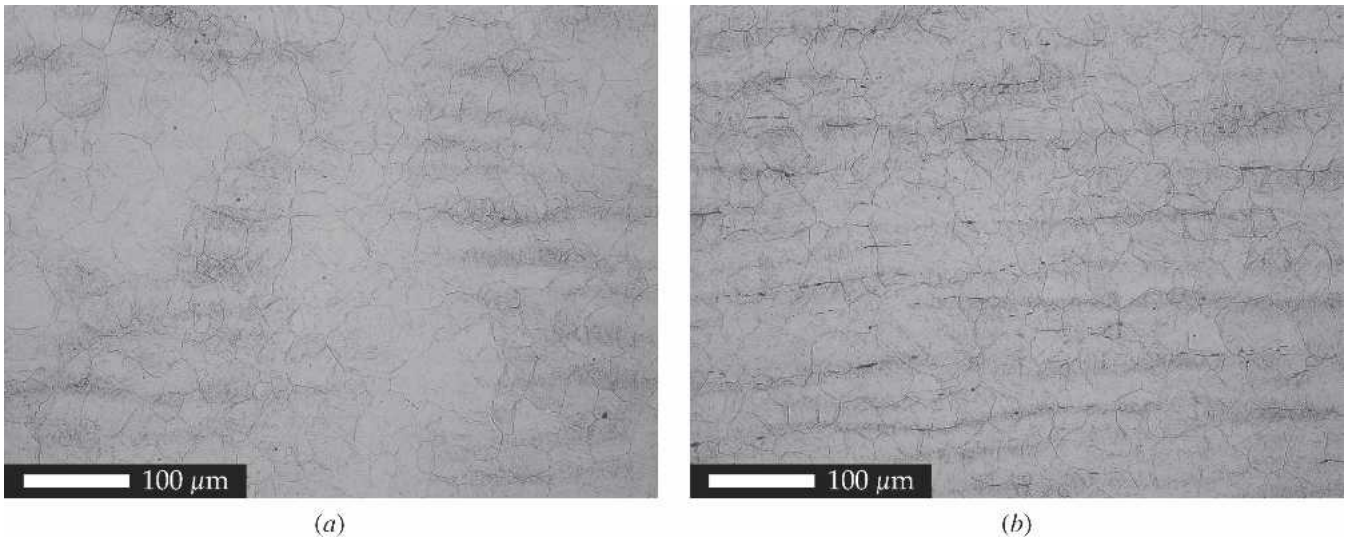

(*a*) (*b*)

Fig. 3—(*a, b*) The microstructure is depicted for low S (LS) material (*a*) and high S (HS) material (*b*) in the longitudinal direction. Also, the former austenite grain boundaries are visible, showing average intercept lengths of 27 μm for the LS and 24 μm for the HS material, in both cases with virtually equiaxed grains. MnSs are naturally visible mainly in the HS material in the layers of the last solidified material (dark contrast).

Table III. Static Mechanical Properties of the Low-S (LS) and High-S (HS) Material in the Longitudinal Direction (L)

Specimen	R_m (MPa)	$R_{p0.2}$ (MPa)	A_5 (pct)	Z (pct)	E (GPa)
average LS-L	1572	1419	8.55	40	191.5
average HS-L	1559	1412	5.89	23	193.5

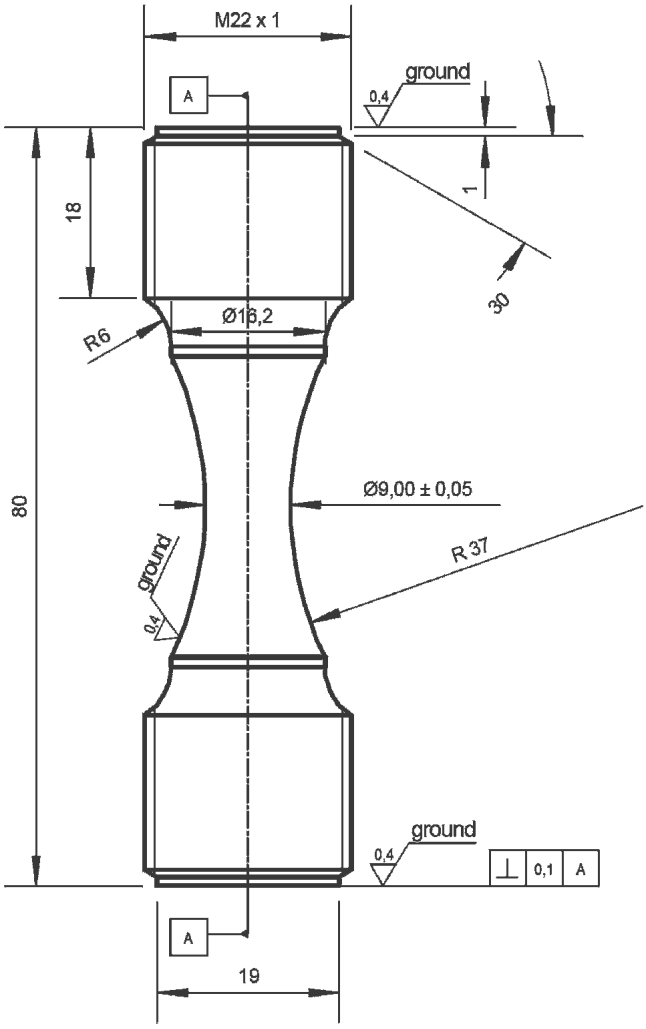

Fig. 4—Geometry of the fatigue push–pull specimen. Subsequent to machining, the surface quality of the center waist area was improved by polishing.

approved (compare with those mentioned previously). The results agree acceptably with the predicted upper and lower boundary fatigue strength (~700 MPa and 300 MPa respectively) for high-speed tool steel SKH51 (450 HV) according to Murakami.[22]

Because Figure 7 comprises data of all four test series, the influence of S and test direction is easy to notice. The increase in S content is responsible for a tremendous drop in fatigue strength. For both the L as well as the S test direction, the fatigue limit plunges some 100 MPa. This drop corresponds to ~18 pct of the fatigue limit for the L and ~28 pct for the S directions. This is a strong indication that an increase in S content will decrease fatigue limits.

Figure 7 emphasizes also the inferior fatigue strength of the S test direction compared with the L direction. This behavior is to see for both the HS as well as for the LS material, where the S values only reach 50 pct of the L values.

Both influences on the fatigue limit—S content and test direction—determine that the test results collect within four scatter bands. It should be mentioned that the scatter bands (mid value ± standard deviation) do not overlap, easing data interpretation and statistically ensuring the result.

For each material and orientation, the probability for fatigue fracture dependent on the stress level was calculated and is depicted in Figure 8. Gaussian distribution of the test results was assumed, thus tests were carried out only in a narrow interval. The fracture probabilities appear as parallel lines in the diagram as a result of similar scatter for all four data series. In the interval from 10 to 90 pct fracture probability, virtually no overlap for the four series can be detected, showing distinct partitioning of the four test series.

D. *Fractography*

As a matter of course, all fracture surfaces of the broken specimens were investigated. Sites of crack initiation were determined as well as the reason for crack initiation. This was, for most specimens, an inclusion, both at the surface of the specimen as well as in the subsurface. This was especially the case for the HS material containing many inclusions. Nearly as many fractures started internally as from the surface, for both the L and the S directions. However, for the LS material, surface initiation was dominant, particularly in the L direction, in which all but one fatigue crack started from the surface. Also, there was, in more than half the cases, no initial inclusion to find.

Figure 9 displays the distribution of inclusion sizes found on the fracture surfaces of the tested specimens. In some cases no ostensible reason for crack initiation was found. These cases were rated as inclusion size <0.01 mm^2 in Figure 9. Depending on the series, between 37 pct and 61 pct of all specimens survived the fatigue test, whereas the remaining samples fractured.

The inclusion areas were measured as the effective area[22] with a smooth contour that envelops the original irregular shape. Depending on the series, 0 to 63 pct of inclusions were smaller than 0.03 mm^2 and could be rated microinclusions. Inclusions with projected area >0.03 mm^2 are called macroinclusions, following DIN 50 602.[23] This is not utterly accurate, because it concerns deformed inclusions but can, according to Murakami,[22] be accepted because only the projected area on the fracture surface is responsible for specimen fatigue failure.

Naturally the defects found in the S direction specimens were according to the orientation of the inclusions much larger than in the L direction, where only the slim cross-section of the defect is ''projected'' onto the fracture surface. The distribution of defect size in Figure 9 reflects this.

The morphology of the inclusions differs widely. Fracture initiation was observed frequently to have started at MnSs clustered with Al_2O_3 (Figure 10). These clusters often have large dimensions. Some clusters did not contain Al_2O_3 but formed extensive grouping of MnSs, which might range over several hundreds of micrometers (Figure 11).

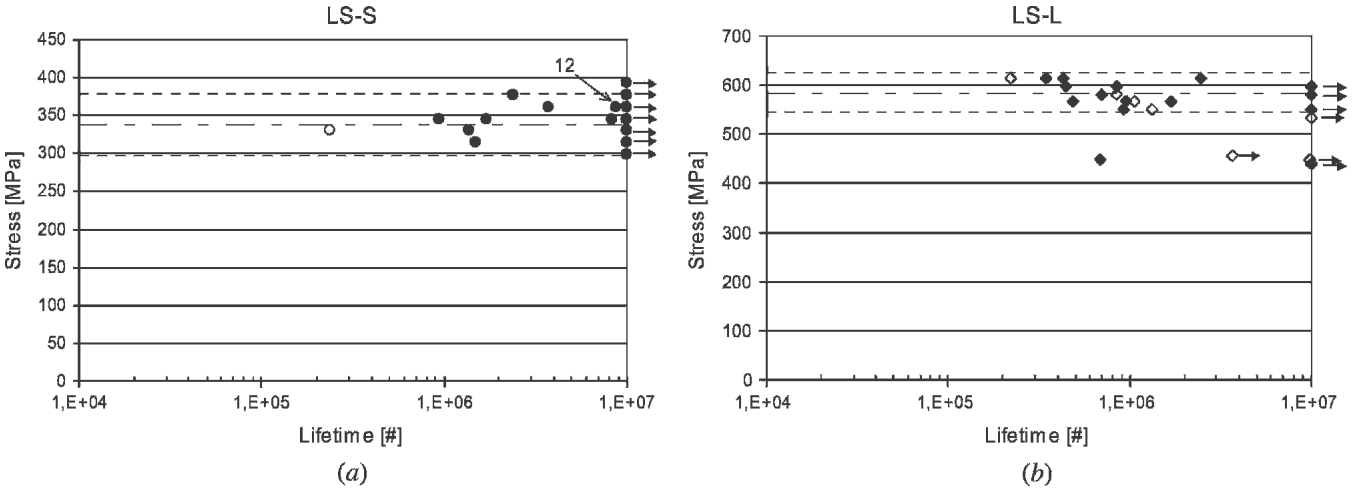

Fig. 5—(*a*) The graph shows a collection of all fatigue test data evaluated on the low-S material short transverse specimens (LS-S). (*b*) The graph gives the collected data for the low-sulfur material longitudinal specimens (LS-L). Data points with blank background have been excluded from the fatigue test results in later consideration (Figure 7). Also, mid values and the interval from the standard deviation are displayed. Stresses are given as nominal stress amplitudes. The data point marked with 12 corresponds to the specimen shown in Figure 12.

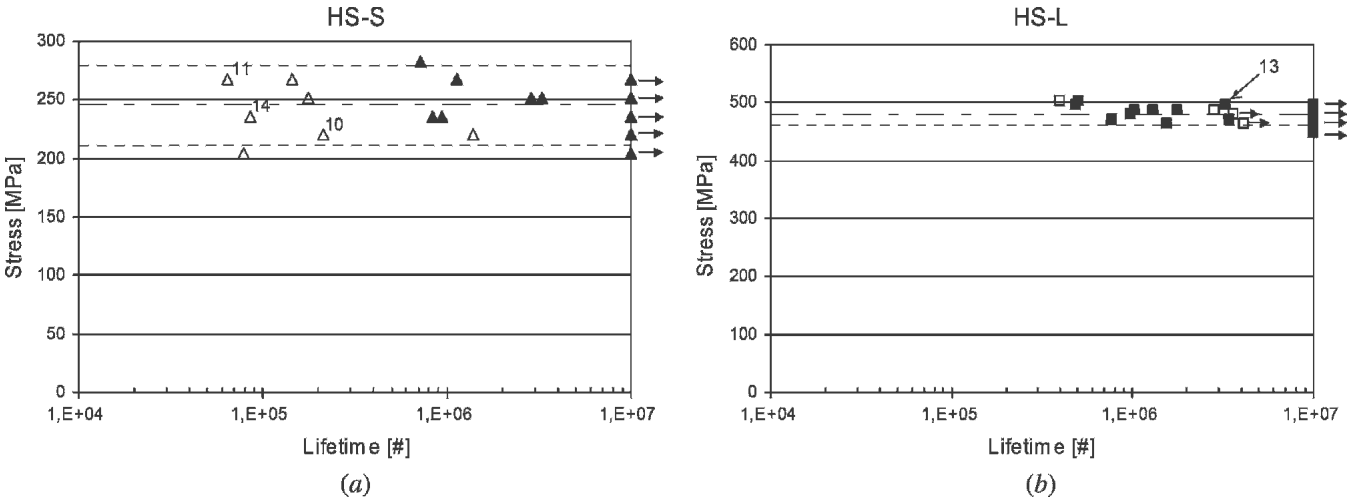

Fig. 6—(*a*) The graph shows a collection of all fatigue test data evaluated on the high-sulfur material short transverse specimens (HS-S). (*b*) The graph gives the collected data for the high-sulfur material longitudinal specimens (HS-L). Data points with blank background have been excluded from the fatigue test results (Figure 7). Also mid values and the interval from the standard deviation are displayed. Stresses are given as nominal stress amplitudes. The data points marked with 10, 11, 13 and 14 correspond to the specimens shown in Figures 10, 11, 13, and 14 respectively.

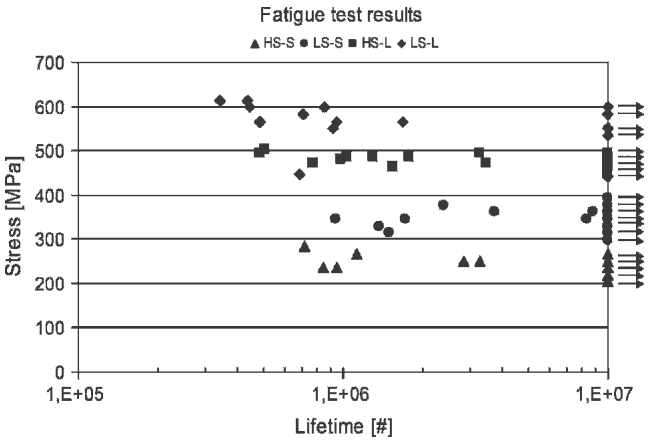

Fig. 7—Collected fatigue test results.

Oxides showed a rather compact appearance (Figure 12), yet some were dispersed spaciously, creating a large effective inclusion size. Widely dispersed oxide inclusions were predominantly found in the LS-S series. Sometimes the boarders of such an inclusion were difficult to define. In the HS material, crack initiations could also be observed from MnS streaks, as shown in Figure 13. These were smaller than the very large MnS clusters, but still far larger than single MnSs.

In two samples, unexpected and extremely large Al-K-Mn-O-S-Si inclusions were found (Figure 14). These were excluded from the modified fatigue test results. Inclusions with a similar chemistry like those giants were also found in smaller dimensions of 0.001 to 0.01 mm^2. One case of crack nucleation on a surface void was found; however, this void originally hosted an inclusion (compare with Figure 14) that was lost either during machining or testing.

Table IV. Mid Value and Standard Deviation for the LS-S, LS-L, HS-S, and the HS-L Series

	Mid Value (MPa)	Standard Deviation (MPa)
LS-S	338	±41
LS-L	585	±40
HS-S	245	±34
HS-L	481	±20
HS-L*	475	±26

Values are given as nominal stress amplitude. LS-L values were calculated with only the last tested 14 data points. HS-L values were calculated with only the last tested 13 data points. HS-L* is a hypothetical result showing mid value and standard deviation calculated with a persistent step size of 7.86 MPa (0.5 kN).

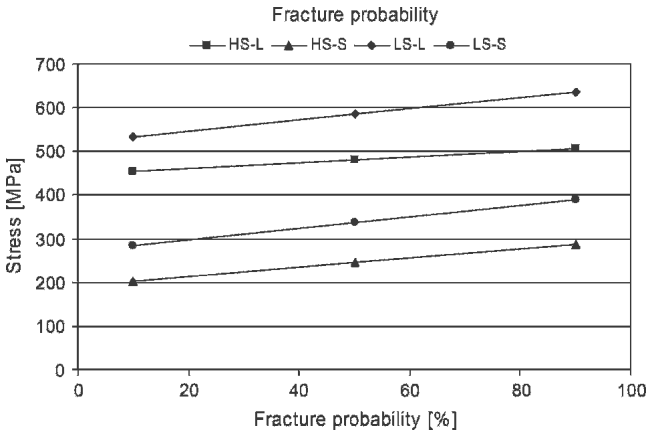

Fig. 8—The graph shows the calculated fracture probability for each material–orientation combination dependent on the applied load. The fatigue test results have been used, assuming Gaussian distribution.

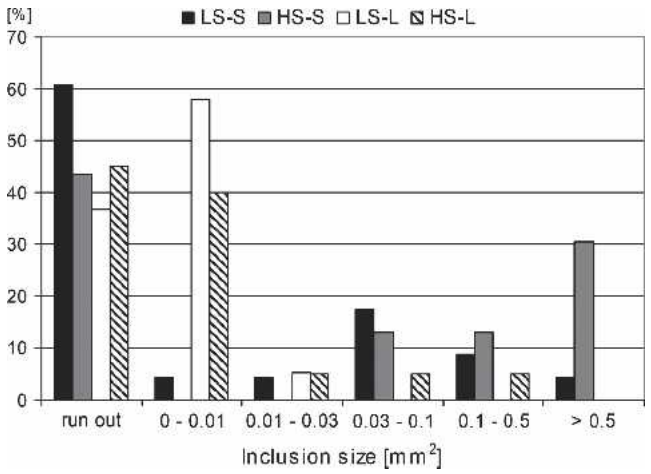

Fig. 9—Detected inclusion size distribution (relative numbers in pct) in the model material. The inclusions are grouped into different intervals. Inclusions <0.03 mm^2 are rated microinclusions.

V. DISCUSSION

The fractography on the fatigue push–pull specimens showed that the steel was not as clean as anticipated. Chemical analysis of the material did not predict the amount, variety, and size of inclusions seen. Comparing the used model material, which was cast in experimental amounts, with commercial production material indicates that also common production material in well-controlled analyses contains large inclusions. Investigations by Sandberg[24] prove, that fatigue fracture on the teeth of gear wheels on countershafts initiate i.a. at inclusions of similar size and type as those in the current investigation. Sandberg[24] documented 15 cases of tooth fractures in case-hardened steel (V-2158-95, Volvo standard) caused by inclusions with sizes of 0.001 to 0.62 mm^2 and of oxide type, most often containing Al, Ca, Mg, and Si. The relative frequency of tooth failures was not provided. This means that for the accomplished experiment, the inclusion population does resemble common situations.

Comparing projected areas of each defect on the fracture surface shows a tendency to large inclusions (>0.03 mm^2) and very large inclusions (>0.5 mm^2) within the HS material (compare with Figure 9). Nordqvist[25] investigated the inclusion distribution in different continuously cast steels. A reason for the inclusion content in continuously cast steel is often the nozzle clogging during the continuous casting

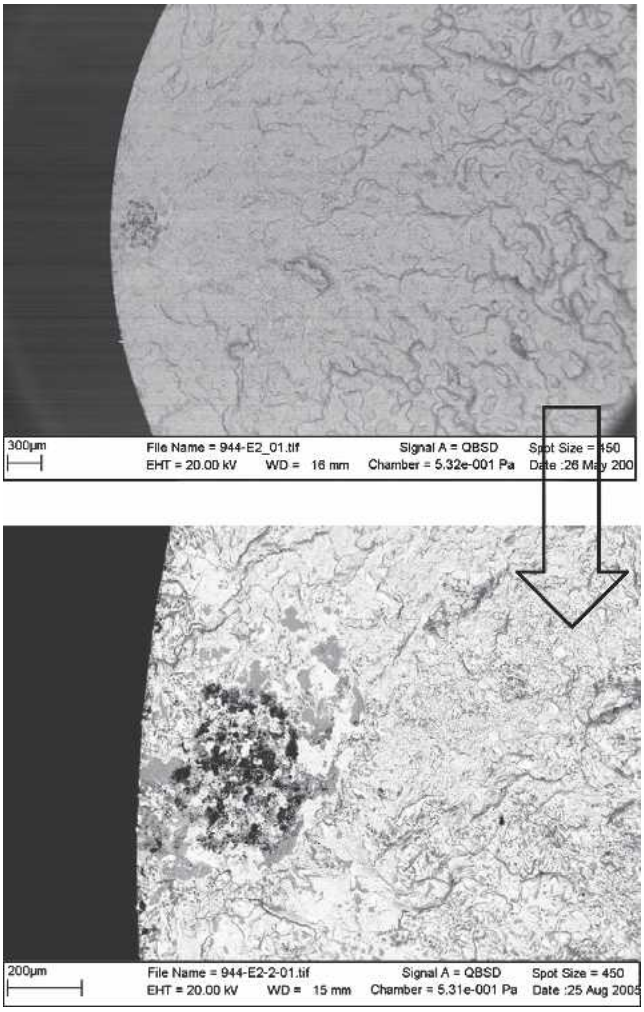

Fig. 10—Crack initiation in an MnS-Al_2O_3 cluster. The dark particles at the edge of the specimen fracture surface are from crushed Al_2O_3. Next to the Al_2O_3 particles are MnSs (dark gray), which solidify on Al_2O_3. The MnSs are excessively flattened.

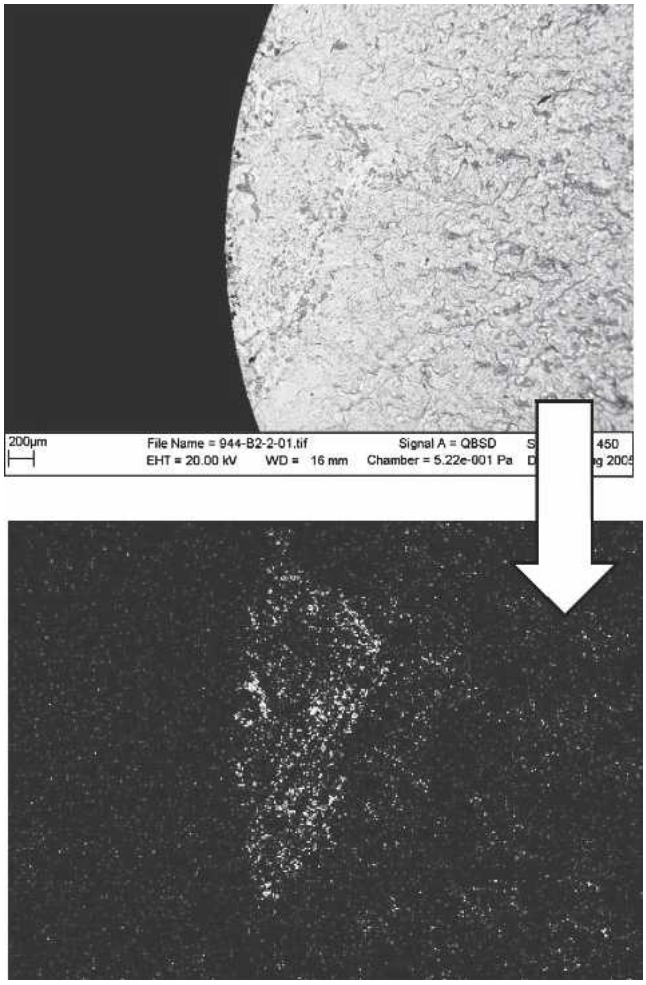

Fig. 11—Fatigue crack initiation at one of the rare ''gigantic'' MnSs. Energy dispersive X-ray analysis (EDX) mapping for S proves the extension of the sulfide.

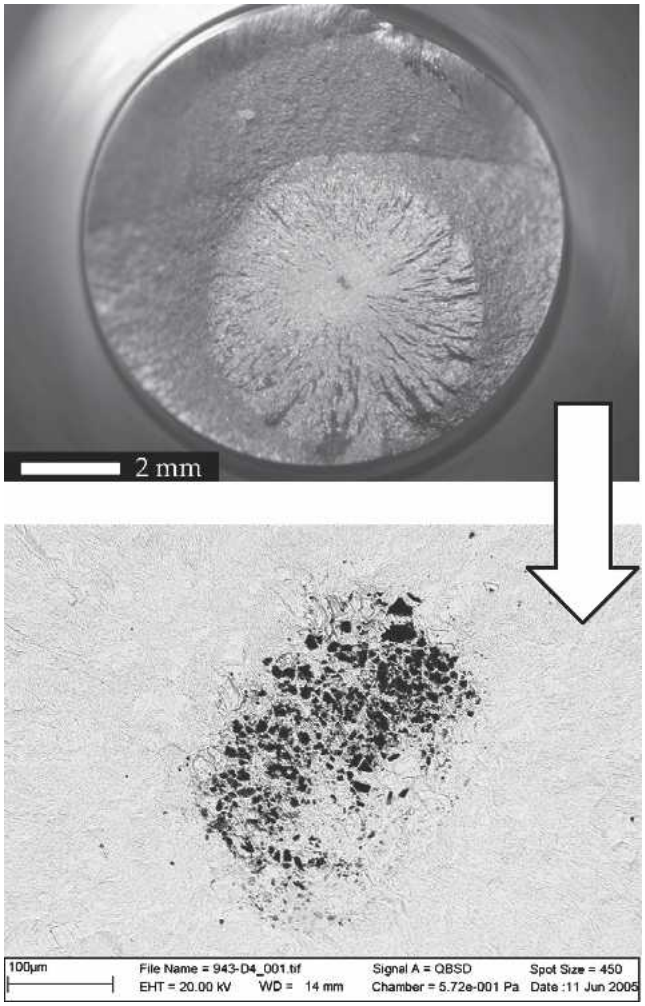

Fig. 12—''Fish eye'' around Al_2O_3. In the back scatter scanning electron microscopy (BS-SEM) image, the (dark) particles of crushed Al_2O_3 are seen. Furthermore, striations can be observed around Al_2O_3.

process. Nordqvist[25] states that higher S content of a material leads to a higher clogging rate from the formation of CaS. When these deposits detach and follow the mold, large inclusions remain in the steel. This happens more frequently in steels with a high S content. Even though the model material was ingot mold cast and S did not form CaS, it shows analog characteristics (*i.e.,* larger inclusions than in a corresponding material with a low S content). For the reasons claimed, the model material is well suited to generate significant and realistic results.

A. *Fatigue Crack Initiation*

Assuming a debonding of the inclusion from the matrix during the first load cycle as an initial stage of fatigue damage,[20,26] as is possible in high-strength steels containing MnS particles, many inclusions act as flaw-like defects already upon initial loading. During fatigue loading, most inclusions discovered develop a sufficient stress intensity range to allow crack growth: $\Delta K \geq \Delta K_{th}$.[27,28] However, several inclusions have dimensions of small cracks, and hence their experienced stress intensity range should not be based on conventional values of ΔK_{th}.[22]

Despite the tendency toward larger inclusions in the HS material (Figure 9), and thus higher local ΔK values, it cannot be assumed that the HS material experiences accordingly shorter life lengths. This can be explained by a higher ΔK_{th} value for material with high inclusion content. Mayes and Baker[4] argue that this phenomenon arises from crack closure effects that are related to the extent of inclusion-induced surface roughening. Indeed, fracture surface roughness is remarkably greater in the HS material compared with the LS material. This variation can be explained with different fatigue crack propagation mechanisms for each material.

B. *Fatigue Crack Propagation*

Although for the LS material a distinct fatigue fracture by conventional striation mechanism (for subsurface inclusions with fish eye) and final rupture can be seen, the differentiation of the fracture characteristics in the HS material is more difficult. This is explained by different crack propagation mechanisms for the two materials. Although a material with a low inclusion content will form a typical

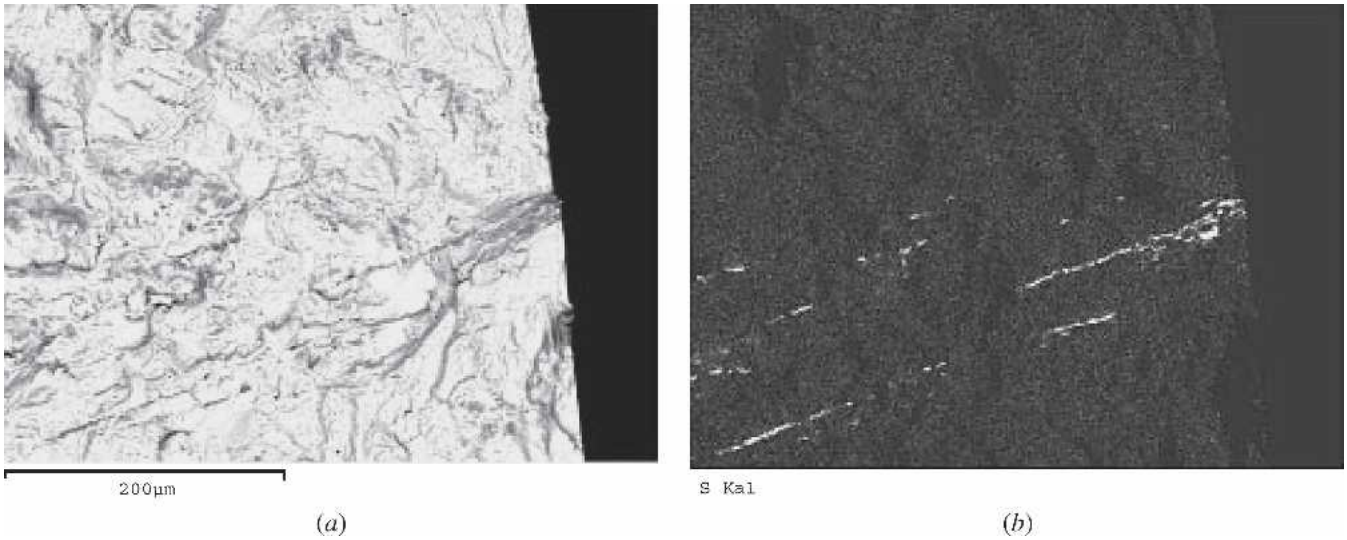

Fig. 13—Fracture from MnS streaks from the surface. (*a*) This image was acquired from a longitudinal specimen using a scanning electron microscope. (*b*) This image is an energy dispersive X-ray analysis (EDX) mapping of the same site, showing the S distribution over the area.

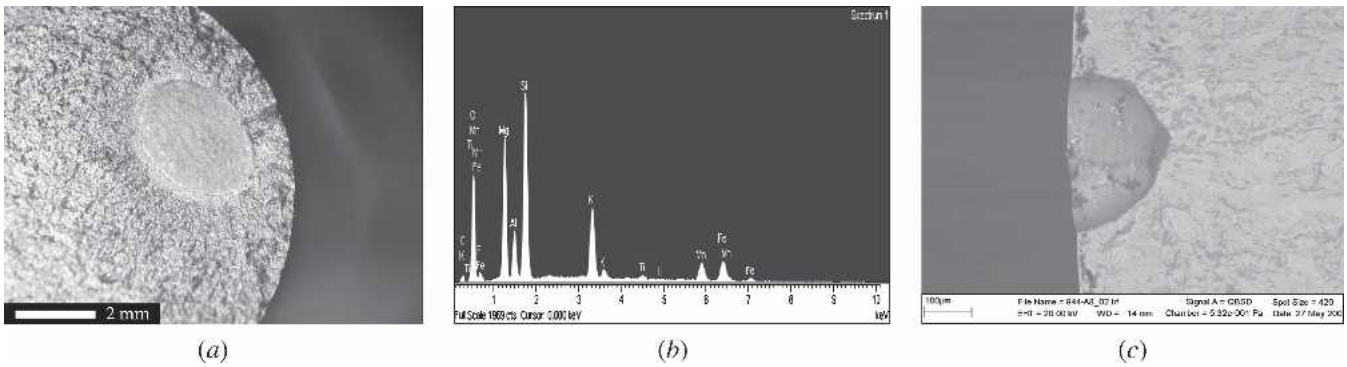

Fig. 14—(*a*) Rare, giant inclusions as the fracture initiation point. Image taken on the fracture surface of a short transverse specimen. (*b*) An energy dispersive X-ray analysis (EDX) spectrum, taken on the inclusion, shows the composition of the Al-K-Mg-O-Si inclusion. (*c*) Crack initiation from a surface void formerly hosting an inclusion of similar type.

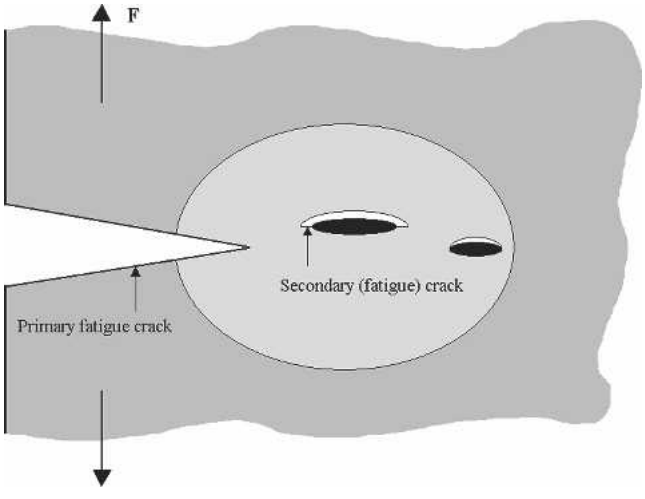

Fig. 15—The stress field in front of the crack tip hosts two inclusions. Interface debonding between inclusion and matrix might occur, which possibly enables secondary fatigue crack growth. Primary and secondary fatigue cracks may link up with a local ductile fracture.

striation pattern, a material with a high inclusion content will produce a different appearance. The interaction between the inclusions and the stress field in front of the crack tip determines the crack growth rate. If there are many inclusions present in this stress field (compare with Figure 15), and they are weakly bonded to the matrix (as assumed for MnS), the interface between the inclusion and the matrix will open,[4,26] thus creating superimposing stress fields. This behavior might introduce secondary (fatigue) cracks around the inclusions,[4] which eventually grow together with the primary crack. Primary and secondary cracks are often offset, which gives rise to the fracture surface roughness. At high ΔK values, the linking between primary and secondary cracks can even occur as a result of local ductile fracture,[29] showing a band of ductility dimples between primary and secondary cracks (compare with Figure 16). Secondary cracking and ductile linking are believed to accelerate the overall fatigue crack growth rate of the HS material compared with the LS material.

The magnitude of the stress concentration at the inclusion in the stress field of the primary crack depends on the

shape of the inclusion. Defects oriented in line with loading will create almost no stress concentration, and thus are not susceptible to debonding of the matrix–inclusion interface and secondary crack growth. However, defects oriented perpendicular to loading generate considerable increase in the stress levels at the tips of the inclusions.

This behavior with secondary cracking enhances with increasing inclusion aspect ratio a/b (where a is the axis perpendicular to and b is the axis parallel to the loading direction). The large difference in stress concentration between longitudinally and short transversally oriented inclusions (in accordance with L and S direction specimens) is a main cause for the substantial amount of fatigue growth anisotropy in forged inclusion-affected steel.

We could not evaluate how large a portion of fatigue life is the result of crack initiation and how much is the result of crack propagation.

Future work aims to find the relation between fracture surface roughness and inclusion content of the material. Quantification of the surface roughness for each test series will allow a determination of crack closure effects and will give further insights into crack propagation mechanisms.

C. *Anisotropy*

The distinct fatigue anisotropy between the S and the L directions for each test material can be learned from Figure 7. The S direction fatigue properties of both materials reach only half the values of the L direction properties.

The differences in fatigue properties between the two materials is not as distinct, but still quite considerable. The LS material performs for the S direction some 38 pct and for the L direction ~22 pct better than the HS material. These values were evaluated with the mid values calculated from the staircase results (Table IV). These mid values seem to describe the material sufficiently well. The standard deviation is, in all cases particularly small, according to the scant scatter in the test results. The modified test results (Figure 7) show the earliest fractures at fatigue lives of ~350,000 cycles and more. Each series had sufficient survivors to verify its fatigue limit.

The relative and absolute anisotropy for each material are evaluated as

$$A_{rel.} = \frac{m_{eS}}{m_{eL}} \qquad [1]$$

$$A_{abs.} = m_{eL} - m_{eS}$$

where m_{eS} = the mid value of test results in S direction and m_{eL} = the mid value of test results in the L direction. The mid values used were determined with the data of the fatigue test results and should point toward a result achieved with fatigue limit values.

The relative anisotropy for the HS material is, with $A_{rel.}^{HS} = 0.51$, somewhat lower (indicating higher anisotropy in the material) than the relative anisotropy for the LS material ($A_{rel.}^{LS} = 0.58$). This means that addition of S and thus an increase in the MnS population within a material does increase the anisotropy of the material. In the case at hand, an increase of S content and thus MnS population by a factor of 10 results in an increase of relative anisotropy of 14 pct. This does not seem much compared with the decreases in fatigue limit by up to 38 pct. The difference in relative anisotropy between the two materials is probably the result of the advantages that crack growth experiences because of elongated MnS in the HS material. LS material crack growth does not have this benefit, and propagation of the crack is not that much easier in the S direction compared with the HS material. The typically larger inclusion size at the crack initiation sites in the HS material are believed to be compensated, at least in part, by the higher ΔK_{th} value.

Also, the absolute anisotropy (corresponding to Eq. 1) is with values of ~236 MPa for the HS material and 267 MPa for the LS material—not differing much.

Höijer[30] performed a similar fatigue anisotropy test on similar material grade with slightly different specimen geometry. Mid values and the relative anisotropies are presented in Table V. Both tests show similar trends, with a lower anisotropy for the LS material. However, anisotropy is generally lower in the material used by Höijer.[30] It is believed that the higher amount of oxides found in Höijer's[30] material is responsible for the smaller amount of directionality. Oxides, which stay more compact during the hot forming operation, do not promote anisotropy as much as MnS clusters in colony with oxides. The high value of relative anisotropy for Höijer's[30] LS material may be the result of the rather moderate result of this test with high scatter and therefore an imprecise mid value.

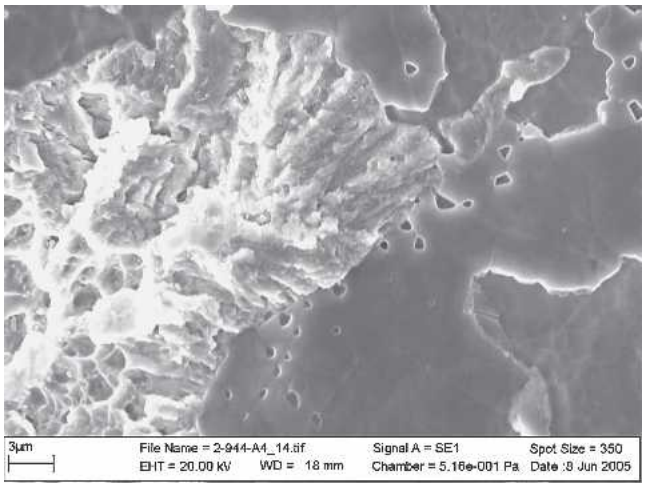

Fig. 16—Secondary fatigue crack at an MnS inclusion with ductility dimples between the primary and secondary cracks. The primary fatigue crack arrived from the left. At the border of the MnS, the secondary fatigue crack can be seen. The lower left corner shows ductility dimples from ductile linking of primary and secondary fatigue cracks.

Table V. Comparison of Existent Test Results and Relative Anisotropy with Those of Höijer[30]

	Existent Mid Values (MPa)	Anisotropy	Höijer's Mid Values (MPa)	Anisotropy
LS-S	338	0.58	358	0.70
LS-L	585		511	
HS-S	245	0.51	275	0.55
HS-L	481		497	

VI. CONCLUSIONS

Anisotropy in fatigue behavior was investigated. The model material was an experimental low-alloyed carbon steel (42CrMo4 steel) with two different S levels: 0.004 wt pct and 0.042 wt pct. The cast materials were cross-rolled to a reduction in thickness of 4.5, leading to flattened MnS inclusions with in-plane rotational symmetry. Subsequent hardening and tempering was performed to give a hardness of HV30 = 450HV, equal in both materials. The fatigue limit levels were then investigated in the L and S directions. The fractographic appearance was related to the amount, shape, and size of the MnS inclusions in the actual test bars.

The following conclusions can be drawn:

1. The LS material shows for both the S and L directions superior fatigue behavior.
2. Both LS and HS materials exhibit marked anisotropy in fatigue behavior. In both cases, the fatigue limit values lie roughly 50 pct lower in the S direction compared with the L direction. However, the HS material shows somewhat more pronounced anisotropic behavior, which can be attributed to the higher MnS population.
3. The recorded scatter around the fatigue limit levels for each condition is relatively limited, safely ranging the fatigue limits of the materials in increasing order: HS-S, LS-S, HS-L, and LS-L.
4. The lower fatigue limits in the HS materials are attributed to the large amount and large size of the fracture initiating MnS inclusions. Easy interfacial decohesion of the MnS inclusions and steel matrix, especially in transverse loading, enhances this behavior.
5. Secondary cracks can form around MnSs. An interconnection of primary and secondary cracks leads to a pronounced fracture surface roughness. This interconnection of primary and secondary cracks (often in a ductile manner) can accelerate fatigue crack growth, whereas the fracture surface roughness may retard fatigue failure.
6. In the LS material with a limited MnS population, the fatigue fracture surfaces are smoother and are characterized by conventional striation patterns.
7. The frequency of MnS inclusions on the final fracture surfaces is pronounced in specimens loaded in the S direction, being a consequence of the relatively easy interfacial decohesion of the inclusions.

ACKNOWLEDGMENTS

Supported by Marchal National Research School for Materials Science funded by Knowledge Foundation Sweden and by Volvo Powertrain Corporation. Future financial promotion is granted by VINNOVA Program Board for Automotive Research.

REFERENCES

1. C. Kaynak, A. Ankara, and T.J. Baker: *Mater. Sci. Technol. (UK)*, 1996, vol. 12, pp. 557-62.
2. R. Kiessling: *Nonmetallic Inclusions and Their Effects on the Properties of Ferrous Alloys*, in *Encyclopedia of Materials: Science and Technology*, Bernhard Ilschner, ed., Elsevier Science Ltd., Oxford, UK, 2001, pp. 6278-83.
3. W.C. Leslie: *ISS Trans.*, 1983, vol. 2, pp. 1-24.
4. I.C. Mayes and T.J. Baker: *Mater. Sci. Technol.*, 1986, vol. 2, pp. 133-39.
5. E. Doege: *Einfluss des Faserverlaufes auf die Schwingfestigkeit und die mechanischen Eigenschaften eines unlegierten Vergütungsstahls in Abhängigkeit vom Schwefelgehalt, Umformgrad und von der Umformtemperatur.* IFUM Do 190/49, Hannover, Germany, 1987.
6. M. Wahlster, H. Heimbach, and K. Forch: *Stahl und Eisen*, 1969, vol. 89, pp. 1037-44.
7. Haglund, S: *Jernkontoret*, Verein Deutscher Eisenhüttenleute, Düsseldorf, Germany, 2004, pp. 4:4-23.
8. T.J. Baker, K.B. Gove, and J.A. Charles: *Met. Technol.*, 1976, vol. 3, pp. 183-93.
9. R. Kiessling and N. Lange: *Non-metallic Inclusions in Steel (Parts –IV)*, 2nd ed., The Metals Society, London, 1978, pp. 114-27.
10. F. Matsuno, S.I. Nishikida, and H. Ikesaki: *Trans. Iron Steel Inst. Jpn.*, 1985, vol. 25, pp. 989-98.
11. A. El-Ghazaly: *Neue Hutte (Germany)*, 1992, vol. 37, pp. 399-404.
12. W.B. Morrison: *Metals Technology*, 1975, pp. 33-41.
13. A.D. Wilson: "Characterization of Inclusions in Plate Steels and Their Influence on Mechanical Properties. Inclusions and their Influence on Material Behavior," ASM International, Chicago, 1989.
14. D. Brooksbank and K.W. Andrews: *J. Iron Steel Inst.*, 1969, vol. 207, pp. 474-83.
15. D. Brooksbank and K.W. Andrews: *J. Iron Steel Inst.*, 1972, vol. 210, pp. 246-55.
16. G. Härkegård: *Eng. Fracture Mech.*, 1974, vol. 6, pp. 795-803.
17. ASTM-International: Designation: E 399 - 90, Metals Test Methods and Analytical Procedures, in *Annual Book of ASTM Standards,* ASTM International, West Conshohocken, PA, 2001, pp. 434-37.
18. ASTM-International: Designation: E 1245 - 03, Standard Practice for Determining the Inclusion or Second-Phase Constituent Content of Metals by Automatic Image Analysis, in *Annual Book of ASTM Standards,* ASTM International, West Conshohocken, PA, 2003, pp. 1-8.
19. G.F. Vander Voort: in *Bearing Steels: into 21st Century, ASTM STP 1327*, J. Joseph J.C. Hoo, and Willard B. Green, eds., ASTM, West Conshohocken, PA, 1998, pp. 13-26.
20. S.B. Hosseini: *Bonding Between MnS Inclusions and the Steel Matrix,* Chalmers Univ. Tech., Göteborg, Sweden, 2005.
21. W.J. Dixon and A.M. Mood: *J. Am. Stat. Assoc.*, 1948, vol. 43, pp. 108-26.
22. Y. Murakami: *Metal Fatigue: Effects of Small Defects and Nonmetallic Inclusions*. Elsevier, Amsterdam, 2002, p. 369.
23. DIN-50602-1985, Beuth Verlag GmbH, ed., Berlin, Germany, 1985, pp. 1-9.
24. F. Sandberg: *Examination of tooth fractures on countershafts (2nd gear) due to fatigue initiated from micro- and macro inclusions, with or without overheating of dedendum flanks, P/N 1521411 & 1521930.* ER-505825 (Volvo Internal Report). Volvo Powertrain, Göteborg, Sweden, 2003.
25. M. Nordqvist: *Steel Cleanliness: Evaluation of Immersion Ultrasonic Testing and Examination of Detected Inclusions.* 2003.
26. S. Suresh: *Fatigue of Materials,* 2nd ed., Cambridge University Press, 2004, p. 679.
27. ASM-International: *ASM Handbook,* 1st ed., ASM International, 1996.
28. N.E. Dowling: *Mechanical Behavior of Materials,* 2nd ed., Prentice Hall, Upper Saddle River, NJ, 1999.
29. A.D. Wilson: *Fractographic Characterization of the Effect of Inclusions on Fatigue Crack Propagation. Fractography and Materials Science,* Williamsburg, VA, 1981, pp. 166-86.
30. J. Höijer: *Anisotropic Fatigue Properties of Engineering Steel: A Microstructural Characterisation.* Chalmers Reproservice, Göteborg, Sweden, 2003.